Stimulation-induced increases in cerebral blood flow and local capillary vasoconstriction depend on conducted vascular responses

Changsi Cai[a], Jonas C. Fordsmann[a], Sofie H. Jensen[b], Bodil Gesslein[a], Micael Lønstrup[a], Bjørn O. Hald[a], Stefan A. Zambach[a], Birger Brodin[b], and Martin J. Lauritzen[a,1]

[a]Center for Neuroscience, Faculty of Health and Medical Science, University of Copenhagen, 2200 Copenhagen N, Denmark; and [b]Department of Pharmacy, University of Copenhagen, 2200 Copenhagen N, Denmark

Edited by Marcus E. Raichle, Washington University in St. Louis, St. Louis, MO, and approved May 10, 2018 (received for review May 10, 2017)

Functional neuroimaging, such as fMRI, is based on coupling neuronal activity and accompanying changes in cerebral blood flow (CBF) and metabolism. However, the relationship between CBF and events at the level of the penetrating arterioles and capillaries is not well established. Recent findings suggest an active role of capillaries in CBF control, and pericytes on capillaries may be major regulators of CBF and initiators of functional imaging signals. Here, using two-photon microscopy of brains in living mice, we demonstrate that stimulation-evoked increases in synaptic activity in the mouse somatosensory cortex evokes capillary dilation starting mostly at the first- or second-order capillary, propagating upstream and downstream at 5–20 μm/s. Therefore, our data support an active role of pericytes in cerebrovascular control. The gliotransmitter ATP applied to first- and second-order capillaries by micropipette puffing induced dilation, followed by constriction, which also propagated at 5–20 μm/s. ATP-induced capillary constriction was blocked by purinergic P2 receptors. Thus, conducted vascular responses in capillaries may be a previously unidentified modulator of cerebrovascular function and functional neuroimaging signals.

conducted vascular responses | pericytes | neurovascular coupling | purinergic signaling | cerebral capillaries

Brain function emerges from signaling in and between neurons and astrocytes, causing fluctuations in the cerebral metabolic rate of oxygen and cerebral blood flow (CBF). Normal brain function depends on a preserved supply of glucose and oxygen, which is mediated by neurovascular coupling, the robust coupling between brain activity and CBF. Neurovascular coupling depends on the functional properties of the association of brain microvessels, astrocytes, pericytes, and neurons, which together constitute the neurovascular unit (1).

Brain arterioles are traditionally thought to control CBF and brain capillaries to serve in the exchange of substances between the blood and brain. This view of CBF dynamics was revolutionized recently by the discovery that both arterioles and capillaries take part in substance exchange (2) and cerebrovascular resistance (3, 4). Specifically, modified smooth muscle cells called pericytes are attached to capillaries and can regulate CBF at the capillary level (3, 5, 6). However, this regulation is not completely understood. Retinal pericytes are constricted by ATP and dilated by neurotransmitters in vitro (5), and they constrict in vivo following stroke (7). In response to light stimulation, retinal capillaries actively dilate and regulate blood flow independent of arterioles (8). Furthermore, glial Ca^{2+} signaling regulates capillary, but not arteriole, blood flow in both the retina and the cerebral cortex (8, 9). Nevertheless, capillary pericytes have been suggested to not be contractile, and that the regulation of CBF in the CNS is only mediated by smooth muscle cells in penetrating arterioles (p.a.s) and capillaries, but not by pericytes on capillaries (10–12). This controversy may be more apparent than real because it depends on how a pericyte and capillary are defined rather than the role of brain capillaries in cerebrovascular control. We have chosen to analyze the change in brain capillaries based on the branching order from the p.a. (13). Using this unbiased methodology, our study may contribute to understanding the contribution of capillaries and pericytes to cerebrovascular control and the interplay between capillaries and arterioles.

All capillaries have pericyte coverage (14), and pericytes are almost completely covered by astrocyte end-feet (15), which raises the possibility that soluble signal molecules released into the microenvironment by astrocytes are sensed by specialized surface receptors on pericytes. ATP is the main transmitter by which astrocytes communicate with neighboring astrocytes (16), as well as an important paracrine transmitter in signaling to neurons (17) and possibly pericytes (18). Therefore, an important part of this study was an examination of the effect of ATP on brain capillary pericytes in vivo.

The current study used in vivo two-photon microcopy of a transgenic mouse model with fluorescent pericytes. The activity-dependent increase in synaptic activity was examined to determine whether capillaries of all branching orders are dilated or constricted, or only capillaries close to the p.a., and whether capillaries exhibit conducted vascular responses (CVRs) similar to pial arterioles.

Our study supports the notion that pericytes play active roles in neurovascular coupling. Furthermore, the results suggest that both arterioles and capillaries contribute to cerebrovascular control during physiological stimulation, and that spatially restricted CVRs may contribute to regulating the flow in brain capillaries and the spatiotemporal characteristics of functional neuroimaging signals.

Significance

Pericytes are located at the outside wall of capillaries. However, whether and how pericytes are involved in the regulation of blood flow in brain capillaries is still debated. We report that capillary vascular responses are mostly initiated and peak at near-arteriole capillaries. These vascular responses are conducted along capillaries at a speed of 5–20 μm/s. Conducted vascular responses in brain capillaries appear to involve pericytes, the mural cells of microvessels, and may be a novel modulator of vascular function in the brain.

Author contributions: C.C., B.B., and M.J.L. designed research; C.C., J.C.F., S.H.J., M.L., and S.A.Z. performed research; C.C. and B.G. contributed new reagents/analytic tools; C.C. and B.O.H. analyzed data; and C.C., B.O.H., and M.J.L. wrote the paper.

The authors declare no conflict of interest.

This article is a PNAS Direct Submission.

[1]To whom correspondence should be addressed. Email: mlauritz@sund.ku.dk.

This article contains supporting information online at www.pnas.org/lookup/suppl/doi:10.1073/pnas.1707702115/-/DCSupplemental.

Published online June 4, 2018.

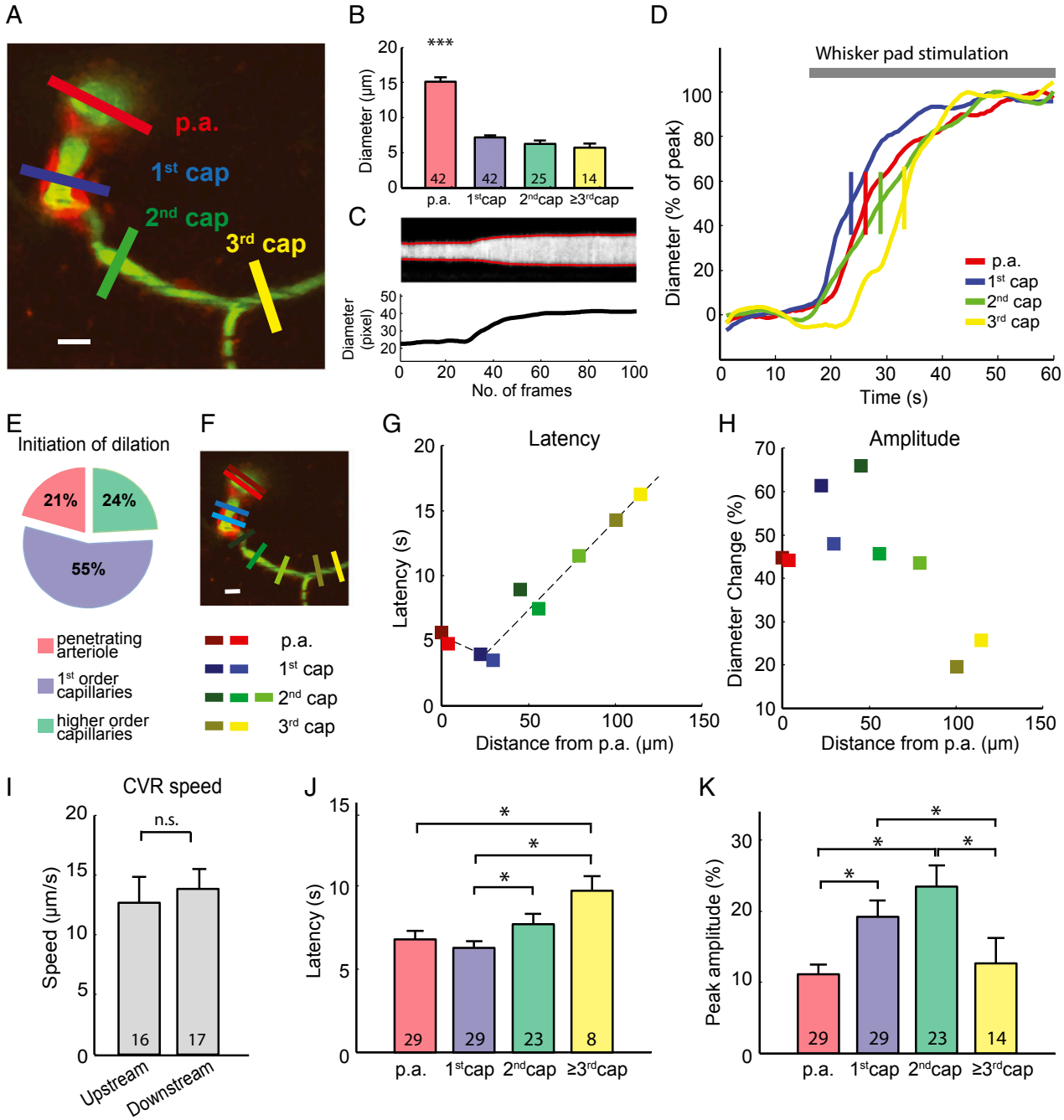

Fig. 1. Functional vessel dilation in the mouse barrel cortex. (*A*) A two-photon image of the barrel cortex of a NG2-DsRed mouse at ~150 μm depth. The p.a.s branch out a capillary horizontally (first order). Further branches are defined as second- and third-order capillaries. Pericytes are labeled with a red fluorophore (NG2-DsRed) and the vessel lumen with FITC-dextran (green). ROIs are placed across the vessel to allow measurement of the vessel diameter (colored bars). (Scale bar: 10 μm.) (*B*) Vessel diameters at different orders of capillaries. p.a., 15.09 ± 4.15 μm; 1st cap (first-order capillaries), 7.18 ± 1.93 μm; 2nd cap (second-order capillaries), 6.25 ± 2.43 μm; 3rd cap (third-order capillaries), 7.63 ± 2.47 μm. The p.a. diameter is significantly larger than all orders of capillaries. ***$P < 0.001$, one-way ANOVA with post hoc test. (*C*) Example trace of fluorescent intensity over time at the blue ROI in *A* is shown as the gray image, and the two red curves indicate the vessel wall (*Upper*). The distance of the two red curves is calculated as the time course of vessel diameter (*Lower*). (*D*) The normalized diameter change over time at different orders of capillaries in response to whisker-pad stimulation. The short vertical bar is where the curve reaches 50% peak, which is defined as response onset. (*E*) Distribution of the locations where the functional dilation initiated ($n = 29$ locations). (*F*) Multiple ROIs at the p.a. and first-, second-, and third-order capillaries are marked as red, blue, green, and yellow, respectively. (Scale bar: 10 μm.) (*G*) In this mouse experiment, the half-maximal dilation latency of each ROI is plotted with corresponding colors on the left along the geographic distance from the p.a. Dashed lines show the linear fit of the conducted dilation. (*H*) The maximal dilation amplitude is plotted with corresponding colors on the left along the geographic distance from the p.a. (*I*) Eighteen out of 29 imaged vasculatures exhibited conducted functional dilation, with an upstream conductive speed of 12.65 ± 0.96 μm/s and downstream conductive speed of 12.83 ± 0.64 μm/s. No significant difference was found between upstream and downstream conductive speeds. n.s., not significant; $P > 0.05$, unpaired *t* test. (*J*) Time to 50% maximal dilation was significantly longer in the third-order capillaries than the p.a. and first-order capillaries. The second-order capillaries dilated significantly slower than the first-order capillaries. *$P < 0.05$, one-way ANOVA with post hoc test. (*K*) Maximal dilation amplitude in different order capillaries. First- and second-order capillaries exhibited significantly larger responses than other locations. *$P < 0.05$, one-way ANOVA with post hoc test. All error bars represent SEM.

Results

CVRs Initiate at Capillaries or p.a.s. We used in vivo two-photon microscopy to image the vasculature in the whisker-barrel cortex of anesthetized mice expressing DsRed in pericytes under control of the NG2 promotor. FITC-dextran was used to label the blood plasma (shown as green in Fig. 1*A*). The p.a.s were identified unequivocally in vivo by tracing their connections back to the pial arterioles and by the clear continuous rings of smooth muscle around them. Only p.a.s with a longitudinal axis perpendicular to the x–y plane were used for data analysis. Capillaries were identified as microvessels branching off from the p.a. with a longitudinal axis parallel to the x–y plane. This geometric arrangement was necessary for reliable measurement of changes in the arteriolar and capillary diameter. Pericytes were identified as NG2-positive mural cells on capillaries branching off from the arteriole. Pericyte cell bodies were spatially separated from the p.a. and each other, and individual pericytes were identified by processes extending longitudinally along capillaries (Fig. 1*A*).

Based on z-stacks of the cortex, we segmented the blood vessels by branching order, 0 being the p.a., 1 being the first-order capillary branching off the arteriole, and so on (Fig. 1*A*). In the resting state, the diameters of the p.a. and first-, second-, and third-order capillaries were 15.09 ± 0.10 μm, 7.18 ± 0.04 μm, 6.25 ± 0.10 μm, and 6.75 ± 0.28 μm, respectively. The p.a. was significantly wider than the capillaries, but the capillary diameter was similar among the first three orders of capillaries (Fig. 1*B*).

Reportedly, first-order capillaries dilate first in response to somatosensory stimulation and the time to vasodilation in first-order capillaries commonly precedes dilation in the p.a. (3). In the present study, the time resolution did not allow us to assess differences in the time of onset of the stimulation-induced vasodilation, but as a proxy we used the latency from stimulus onset to 50% maximal dilation (Fig. 1*D* and Movie S1). Out of 29 preparations, stimulation-evoked dilation was achieved first in first-order capillaries in 55% of experiments, whereas dilation was achieved first in the p.a. in 21% and in second- or third-order capillaries in 24% of experiments (Fig. 1*E*). Next, we evaluated whether a pattern exists in the development of capillary dilation, that is, whether dilation occurs first at a particular point and whether the reaction spreads according to the branching order of the capillaries. For this purpose, multiple regions of interest (ROIs) rectangles with the long side perpendicular to the vessel wall were drawn as indicated by the color coding in Fig. 1*F*. The half-maximal latency and maximal vascular dilation for each ROI was plotted as a function of the geographic distance along the vasculature from the p.a. using the same color coding as the squares representing ROIs (Fig. 1 *G* and *H*). Fig. 1*G* shows the x–y plane of one mouse. Dilation initiated at the first-order capillary, and the dilation propagated to the p.a. and second and third capillaries in a linear fashion. The first- and second-order capillaries demonstrated the strongest dilation (Fig. 1*H*). The time sequence of vascular reactions could be reported for 18 of the 29 experiments; in 11 experiments the baseline stability was suboptimal. In the experiments with a stable enough baseline, the averaged upstream conductive speed was 12.65 ± 0.96 μm/s and averaged downstream conductive speed was 12.83 ± 0.64 μm/s (Fig. 1*I*). The vascular dilation spread with the same velocity upstream and downstream ($P = 0.67$). Dilation was significantly slower in the second-order and higher capillaries than in the first-order capillaries and the p.a. (Fig. 1*J*), whereas changes in diameter were significantly greater in the first- and second-order capillaries than in the p.a. and higher-order capillaries (Fig. 1*K*).

To exclude the possibility that the conducted responses were affected by focus drift, we carried out hyperstack imaging (continuous and repetitive recordings of z-stack images) during whisker-pad stimulation. Images were flattened to produce a time-series movie by maximum intensity projections for each image stack. This procedure confirmed CVRs in the p.a.s and capillaries upon whisker stimulation, both upstream and downstream, in five of five experiments (*Supporting Information*, Fig. S1, and Movie S2).

CVRs Induced by Local ATP Injection. Purinergic signaling may affect the neurovascular unit in pathological states, such as during cerebral ischemia when ATP is released in high concentrations (19–22). ATP constricts retinal pericytes and capillaries in vitro, which is of interest because brief periods of ischemia lead to the no-reflow phenomenon and a reduction in the caliber of small vessels (7, 23). We examined the effect of purinergic receptor activation on pericytes and capillaries in vivo by local injection of ATP into the barrel cortex of NG2-DsRed mice. Guided by the two-photon microscope, a glass micropipette was inserted into the cortex and advanced to close proximity of the p.a. and the first few orders of capillaries. A mixture of 10 μM Alexa 594 (red color in the glass micropipette) and 1 mM ATP was puffed from the micropipette by air pressure (Fig. 2 *A* and *B*). ATP puffing evoked capillary dilation, followed by constriction (Fig. 2*B* and Movie S3). Fifteen rectangular ROIs were studied at different-order capillaries (Fig. 2*C*) and the normalized diameter change was plotted over time for each ROI (Fig. 2*D*). Amplitudes of dilation or constriction were defined as positive or negative amplitudes at maximal vascular response. The latency of dilations and constrictions were reported as the time to half positive or negative maximum after puffing onset (Fig. 2*E*). The four variables were plotted as a function of the geographic distance along the vasculature from the p.a. (Fig. 2 *F*–*I*). The same color coding was used for the squares representing ROIs. The branching point of the first- to second-order capillary exhibited the strongest and earliest dilation and constriction, whereas the third-order capillary had a very small change in diameter (Fig. 2 *F* and *G*). A significantly higher amplitude of both vasodilation and vasoconstriction was found at the first- and second-order capillaries, whereas the diameters of higher-order capillaries were almost unaltered ($n = 7$; Fig. 3 *A* and *B*). The latencies of vasodilation and vasoconstriction at third-order and higher capillaries were significantly longer than at lower-order capillaries (Fig. 3 *C* and *D*). No significant difference was found for the mean distance from the pipette tip to the different-order capillaries, which excludes an influence of distance to pipette tips on the conducted responses (Fig. 3*E*). Furthermore, traces from individual mice indicated no correlation between pipette distance and the response properties (i.e., latency and amplitude) (Fig. S2).

ATP-puffing-induced dilation and constriction demonstrated linear or near-linear conduction in the upstream and downstream direction (Fig. 2 *H* and *I*). The conductive speed of dilation to upstream and downstream vessels was 11.47 ± 3.37 μm/s and 14.78 ± 3.85 μm/s, respectively, whereas the conductive speed of constriction to upstream and downstream vessels was 6.54 ± 1.05 μm/s and 6.55 ± 1.22 μm/s, respectively, that is, slower than for dilation (Fig. 3*F*). Hyperstack imaging during ATP puffing confirmed conductive responses for both ATP-induced dilation and constriction in five of five experiments (*Supporting Information*, Fig. S3, and Movie S4). The faster conductive speed for downstream dilation suggests that ATP-induced conducted vascular dilation and constriction are modulated by different mechanisms.

ATP-Puffing-Induced Constriction, but Not Dilation, Depended on Purinergic Type 2 Receptors. To probe the mechanism of ATP-puffing-induced constriction, 0.5 mM of the P2 receptor antagonist pyridoxalphosphate-6-azophenyl-2′,4′-disulfonic acid (PPADS) was applied topically to the exposed cortex at least 2 h before ATP puffing. Preconditioning with PPADS preserved vessel dilation but profoundly attenuated vessel constriction (Fig. 4 *A* and *B*). The sensitivity to PPADS was particularly pronounced in first- and second-order capillaries (Fig. 4 *C* and *D*). This indicates that the

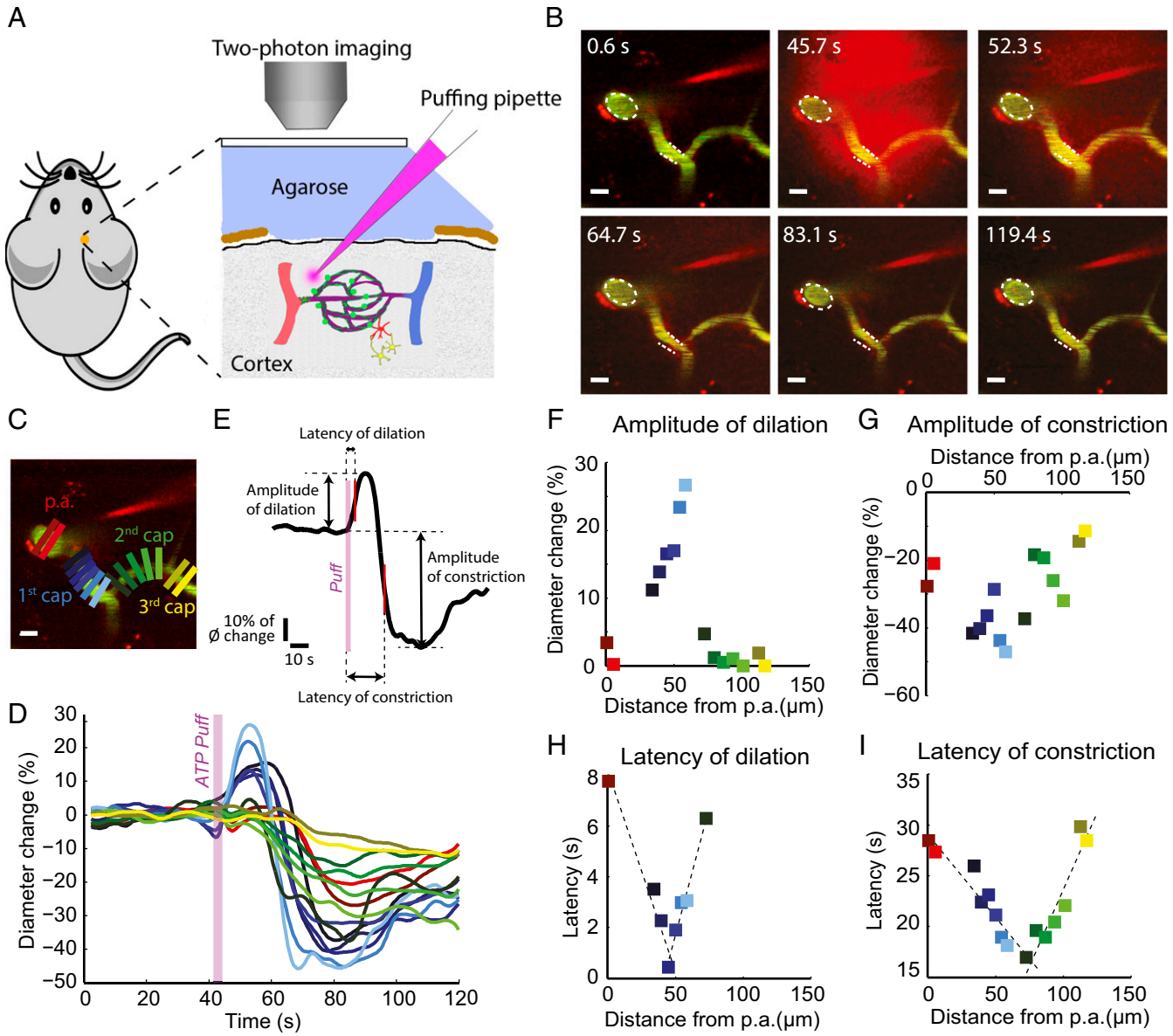

Fig. 2. ATP puffing by micropipette induces vessel dilation, followed by constriction. (*A*) Diagram of the in vivo experimental setup. The puffing micropipette is placed in proximity of the near-arteriole site. The micropipette contains a mixture of 10 μM Alexa 594 (red color in glass micropipette) and 1 mM ATP. (*B*) Video snapshots of the time course of puffing with 1 mM ATP from the micropipette. Vessel dilation precedes constriction. Dashed lines indicate the vessel contours at the resting state. (Scale bars: 10 μm.) (*C*) Multiple uniquely colored ROIs are placed along the vasculature to measure the vessel diameter. (Scale bar: 10 μm.) (*D*) Normalized diameter change is plotted over time for each ROI. The ROIs and trace color are coded identically. (*E*) Amplitudes of dilation or constriction are defined as positive or negative amplitudes at the maximal vascular response. The latencies of dilation and constriction are reported as time to half positive or negative maximum after puffing onset. (*F–I*) In this mouse experiment, the distribution of all ROIs in *C* and *D* with amplitude of dilation (*F*), amplitude of constriction (*G*), latency of dilation (*H*), and latency of constriction (*I*) over the geographic distance from the p.a. along the vasculature. The dashed lines represent the linear fit of the upstream and downstream conductive responses.

ATP-induced constriction observed in the absence of inhibitor at first- and second-order capillaries, and to a lesser extent at the p.a. and third-order and higher capillaries (Fig. 3), was due to P2 purinergic receptor activation.

Activation of both P2X and P2Y Receptors Leads to Similar Vessel Responses. In vitro studies of arteries and arterioles have shown that the activation of P2Y receptors on smooth muscle cells leads to vessel constriction, whereas the activation of P2X receptors on arteriolar endothelial cells (ECs) leads to vessel dilation (24–27). To test whether the same mechanisms contribute to brain capillary control in vivo, we investigated the vessel responses elicited by both P2X and P2Y receptor agonists. P2X receptor agonist αβATP (αβ-methylene-ATP) and P2Y receptor agonist UTP were administered (1 mM each) by puffing in close proximity to the p.a. and the first few order capillaries. As adenosine hydrolyzed from ATP is a potent vasodilator (28), a more stable ATP analog, ATPγS, was used at a concentration of 1 mM for micropipette puffing experiments. Finally, control experiments were performed by puffing 10 μM Alexa 594 only to rule out the effect of puffing itself.

We compared the effect of the compounds on the first-order capillary responses because these capillaries had the most robust and profound responses upon ATP puffing (Fig. 3; see also Fig.

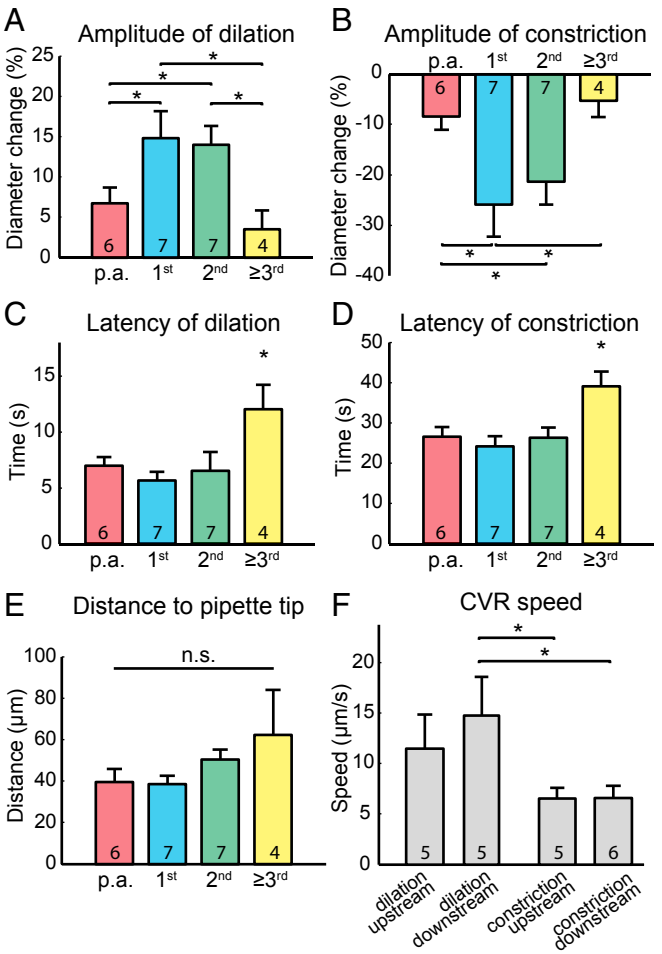

Fig. 3. ATP-puffing-induced dilation and constriction vary in amplitude and latency at different-order capillaries. (*A*) The amplitudes of dilation and (*B*) constriction are significantly higher at first- and second-order capillaries compared with other order capillaries. (*C*) The latencies of dilation and (*D*) constriction are significantly longer for third-order and higher capillaries than other order capillaries. *$P < 0.05$, one-way ANOVA with post hoc test. (*E*) The mean distance from the pipette tip to the vessels of the different branch orders. n.s., not significant; $P > 0.05$, one-way ANOVA with post hoc test. (*F*) Comparison of upstream and downstream conductive speeds of ATP-puffing-induced dilation and constriction. *$P < 0.05$, one-way ANOVA with post hoc test. All error bars represent SEM.

S4). Both P2X and P2Y receptor agonists induced dilation of the first-order capillaries, followed by constriction. Although the amplitudes of dilation were the same for all compounds (Fig. 5*A*), control experiments using only Alexa 594 showed only weak dilation in one of the five experiments. The amplitude of vasoconstriction was significantly larger with ATPγS than ATP (Fig. 5*B*), which could be explained by ATPγS inducing vasoconstriction via activation of both the P2X and P2Y receptors. The dilator effect is less pronounced because ATPγS is more stable than ATP, with the formation of less adenosine. In control experiments, vessel constriction was rarely observed. Both vasodilation and vasoconstriction took longer to develop when evoked by ATP than for the compounds that were more stable (Fig. 5 *C* and *D*). This may be explained by the vasodilator adenosine hydrolyzed from ATP prolonging the latency to maximal vasoconstriction. A comparison of upstream and downstream conductive speeds of both vasodilation and constriction with the four compounds found no significant difference (Fig. 5*E*), suggesting that the four compounds exert the conducted vasoresponses via a similar mechanism.

Instant and Severe Pericyte Constriction After Ischemia. To study the instant response of pericytes in ischemic stroke in vivo, cardiac arrest was induced by i.v. injection of 0.05 mL pentobarbital. An image stack covering the whole near-arteriole region was recorded before cardiac arrest, and another image stack in the same region was recorded 5 min after cardiac arrest. Each image stack was then projected onto one image by average intensity projection. The p.a. and first- and second-order capillaries exhibited severe constriction, in some cases with red blood cells clogged inside, but only adjacent to pericyte cell bodies. The third-order or higher capillaries exhibited less constriction, though they also had mural pericytes (Fig. 6 *A* and *C*). Capillaries with visible pericyte cell bodies exhibited more constriction than capillaries devoid of pericyte cell bodies (Fig. 6*C*).

Next, we evaluated whether purinergic receptors were involved in the ischemia-induced capillary constriction by pericytes. For this purpose, we superfused the exposed mouse cortex with 0.5 mM PPADS for at least 2 h before cardiac arrest. This mitigated constriction of the p.a. and first- and second-order capillaries (Fig. 6 *B* and *C*). These results are consistent with prior studies of brain slices and postmortem studies suggesting that pericytes constrict in ischemia (3, 7) and that preconditioning the animals with PPADS helps in the recovery from experimental stroke (29, 30). We conclude that pericytes at the first several orders of capillaries constrict severely after ischemia in vivo and that blocking purinergic receptors mitigates the constriction of both arterioles and capillaries.

Discussion

Understanding neurovascular signaling in response to neuronal or astrocytic activity is crucial to understanding how brain processes are supplied with energy and functional neuroimaging signals are generated. Our results demonstrate that first- and second-order capillaries initiate functional dilation more often than the p.a. and higher-order capillaries. In addition, local and direct administration of ATP induces vessel dilation, followed by constriction at the first several orders of capillaries. Functional dilation and ATP-puffing-induced dilation and constriction are initiated mostly at the first- or second-order capillaries, and CVRs develop both upstream and downstream. However, the velocity of conducted vasodilation is faster than for conducted vasoconstriction. Furthermore, minutes after cerebral ischemia, pericytes at near-arteriole sites constrict via a P2 receptor-dependent mechanism.

The contribution of pericytes to CBF regulation has been controversial (13). Some in vivo studies suggest a role of pericytes in the regulation of capillary blood flow (3, 6), whereas others have indicated that flow control was detectable only in arterioles, but not in capillaries, and that vascular smooth muscle cells, but not pericytes, contribute to the regulation of CBF responses (10–12). However, most of those studies have suggested that pericytes close to the p.a. are contractile during normal brain activity, and pericytes on first- and second-order capillaries have hybrid features of both smooth muscle cells and capillary pericytes (31). In our studies, pericytes were identified by two-photon microscopy as red-fluorescent cells on the capillary wall in NG2-DsRed mice. Nevertheless, we describe the changes in capillary function according to the branching orders from the p.a. and involvement of pericytes in this context. Our results strengthen the importance of using a defined vessel geometry with respect to the cortical surface to reliably assess small changes in the diameters of capillaries.

Similar to other studies (3, 10), our data suggest a key role of capillaries close to the p.a. in local blood flow control. As a powerful tool for studying CBF (32), the two-photon imaging microscope was

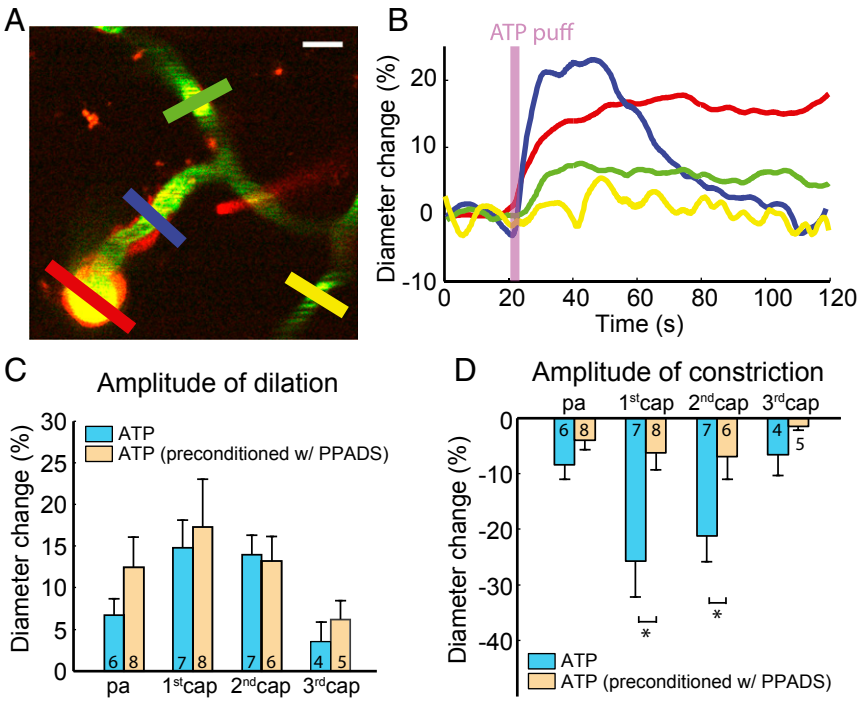

Fig. 4. ATP-puffing-induced constriction is mediated by purinergic type 2 receptors. (*A*) After topical application of 0.5 mM PPADS, the puffing pipette is placed in proximity of a near-arteriole site. Red, blue, green, and yellow ROIs are placed at the p.a. and first-, second-, and third-order capillaries to measure the diameter, respectively. (Scale bar: 10 μm.) (*B*) Time course of the diameter change in each ROI indicated in *A*. Preconditioning with 0.5 mM PPADS and puffing with 1 mM ATP induces dilation but profoundly attenuates constriction. (*C*) The amplitude of dilation is not significantly different with and without the application of PPADS among all orders of capillaries. n.s., not significant; $P > 0.05$, unpaired *t* test. (*D*) The amplitude of constriction is significantly different with and without preconditioning with PPADS on the first- and second-order capillaries. $*P < 0.05$, unpaired *t* test. All error bars represent SEM.

used to focus on one horizontal plane at a depth of 100–200 μm to obtain good image quality. This horizontal plane most commonly included one p.a. and the associated first-, second-, or third-order capillaries. Our results showed that capillary dilation as a response to increased synaptic activity (i.e., the neurovascular coupling response) is initiated in most cases in first-order capillaries. This is consistent with earlier results indicating active relaxation of pericytes before relaxation of arteriolar smooth muscle cells (3), and with recent studies showing that smooth muscle actin is present in pericytes at near-arteriole capillaries (10, 33). In addition, pericytes at near-arteriole capillaries may have denser smooth muscle actin (12, 34), as the first- and second-order capillaries react with the earliest and most profound dilation.

ATP puffing induced dilation and constriction in the first few orders of capillaries. ATP puffing onto higher than second-order capillaries induced almost no changes in diameter. The observations indicate that pericytes have different sensitivities to purinergic stimulation, in accordance with previous studies (5). Dilation induced by ATP puffing has been suggested to be mediated by the activation of P2X receptors on arteriolar ECs (24). However, a recent study proposed that ATP may also act on astrocytic P2X1 receptors to evoke the release of PGE_2, which relaxes pericytes (9). Other studies have shown that the ATP analog ATPγS has its own pharmacological profile; for example, it may in fact be hydrolyzed to adenosine (35), which may be another explanation for ATP-puffing-induced vasodilation.

ATP-puffing-induced vessel constriction was profoundly attenuated by the purinergic type 2 receptor antagonist PPADS, indicating the involvement of purinergic type 2 receptors. Similar to our study, ATP puffing in brain slices was previously shown to increase cytosolic Ca^{2+} in glial cells, followed by adjacent vasoconstriction, which was abolished by preincubation with P2Y1 receptor blocker (36). Our in vitro studies with pericytes in monoculture (*Supporting Information*, Fig. S5, and Movie S5) confirmed that ATP constricted capillary pericytes in a manner dependent on P2 receptor activation and increased cytosolic Ca^{2+}. This study demonstrates that intracellular Ca^{2+} increases in pericytes may be the mechanism underlying pericyte contraction in response to ATP. ATP applied to cerebral arterioles in vitro produced a biphasic vessel response, constriction followed by dilation (24), which is the opposite of what we observed in capillaries. The data suggest that the effect of the purinergic signaling cascade in capillaries is different from the effect in arterioles (9).

In arteries and arterioles, CVRs are primarily characterized by fast (1–3 mm/s) and far-reaching electrical conduction along well-coupled endothelium and into smooth muscle (37, 38). Upon G-coupled receptor stimulation, a secondary slow and spatially limited Ca^{2+} wave spreads along the endothelium (~100 μm/s), giving rise to nitric oxide and prostaglandin production (Fig. 7 *A* and *B*). Inhibition of the electrical component has demonstrated that the speed of the slow, diffusion-based CVR is ~20 μm/s, similar to the slow speed of propagated vasodilation observed in the present study (39). Furthermore, hyperpolarizing pulses propagate along the ECs in capillaries, with a conductive speed 100 times faster than the diffusion-mediated CVR (37). In contrast, the vascular relaxation times are the same for the two types of conducted responses. It is possible that the final common path of both types of vascular responses may involve axon boutons dumping potassium concurrent with rapid spiking (40), but this will need to be addressed in more detail in future studies.

Although the underlying mechanism remains unclear, a diffusion-based conduction of vasomotor responses emanating from first- and second-order capillaries can be envisioned, for example paracrine signaling along astrocytic end-feet or intracellular diffusion across gap junctions connecting ECs and/or pericytes (Fig. 7*C*). However,

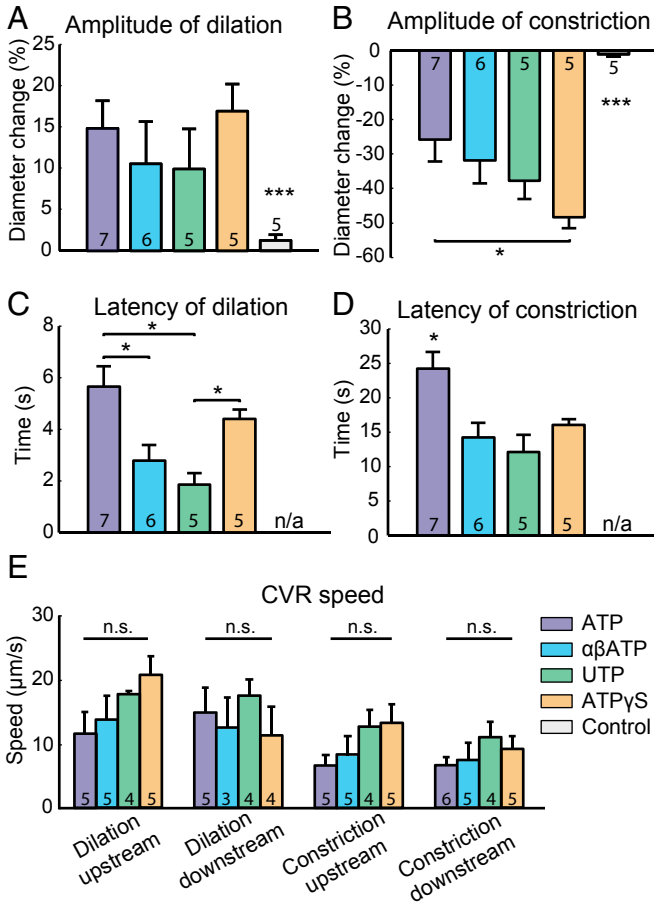

Fig. 5. Vessel responses of first-order capillaries to puffing with ATP, P2X, P2Y receptor agonists, ATPγS, and red dye. (*A*) Comparison of different puffing compounds with amplitude of dilation, (*B*) amplitude of constriction, (*C*) latency of dilation, (*D*) latency of constriction, and (*E*) conductive speed. The compounds are 1 mM ATP, 1 mM P2X receptor agonist (αβATP), 1 mM P2Y receptor agonist (UTP), 1 mM ATPγS, and 10 μM Alexa 594 as control. n/a, not available; $*P < 0.05$, $***P < 0.001$, one-way ANOVA with post hoc test. Note that the latency of the control experiment is marked as not available for both dilation (*C*) and constriction (*D*). This is due to the small responses upon control puffing and the suboptimal measurements of latency. All error bars represent SEM. n.s., not significant.

documentation of gap junction coupling between the ECs of first- and second-order capillaries in mouse cortex is lacking. In addition, in contrast to arterial endothelium, capillary ECs do not harbor SK_{Ca}/IK_{Ca} channels (37), which are thought to underlie the initiation of fast electrical CVRs (41). This may also explain why microapplication of ATP to pial arteries and p.a.s in vitro has been observed to result in constriction followed by endothelium-dependent propagated vasodilation (25, 26).

During ischemia, cerebral pericytes constrict and stop the blood flow in capillaries within a few minutes. The constriction is pronounced at the p.a. and first- and second-order capillaries, whereas the diameters of higher capillaries remained constant. This supports and modifies the notion that pericytes contribute to the long-lasting decrease in capillary blood flow after cerebral ischemia (3, 7, 42). The most ischemia-sensitive region of the vasculature is first-order capillaries at the near-arteriole site. Preconditioning with the P2 receptor antagonist PPADS alleviated pericyte constriction after ischemia, which may be related to the blockade of purinergic type 2 receptors, but its effect in preventing pericyte constriction in ischemia is equally likely to reflect that it blocks the reversed mode of Na^+/Ca^{2+} exchange, a well-known route for Ca^{2+} overload in ischemia (43). Moreover, PPADS blocks ecto-ATPases (44), thereby promoting pericyte constriction after ischemia. Other studies have reported that that modulation of purinergic receptors promotes animal recovery from stroke in vivo (29, 30), but our studies show that pericytes on first-order capillaries can be rescued by blocking purinergic receptors before cerebral ischemia.

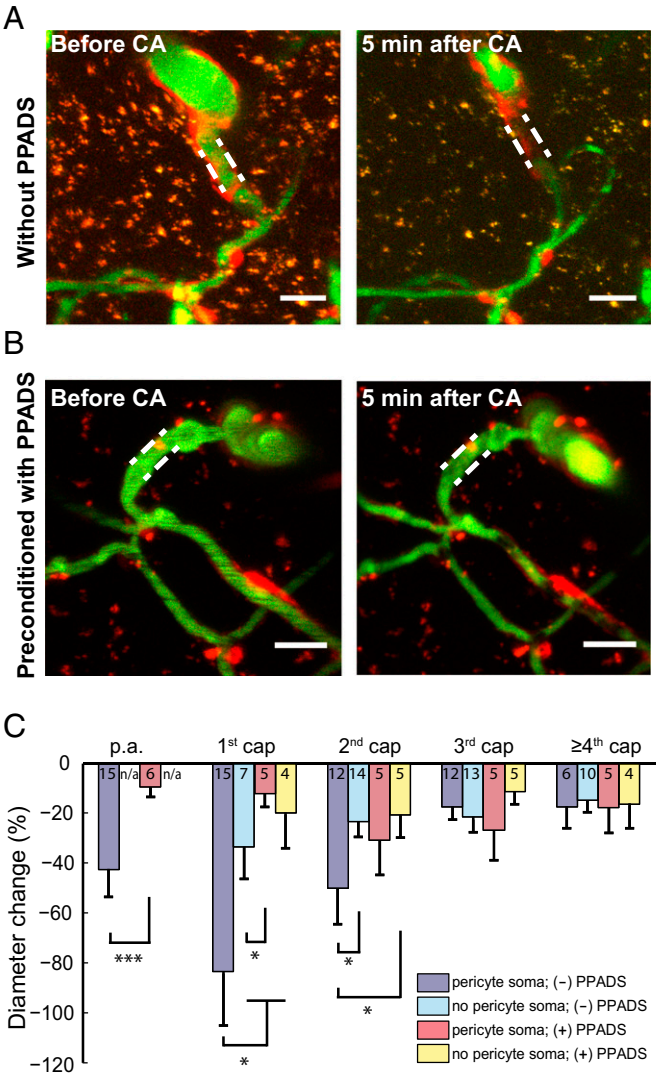

Fig. 6. Ischemia leads to severe constriction of capillaries at the near-arteriole site and preconditioning of P2 receptor blockers mitigates constriction of capillaries. (*A*) Image stacks (1-μm step size, average intensity projection) of the vasculature, including the p.a. and first few orders of capillaries. Five minutes after ischemia by cardiac arrest (CA), severe constriction was observed at the p.a. and first- and second-order capillaries, but third-order and higher capillaries were moderately constricted. Dashed lines indicate the vessel contours of first-order capillaries before cardiac arrest. (Scale bars: 20 μm.) (*B*) Preconditioning with 0.5 mM PPADS for 2 h rescued severe constriction of the p.a. and first-order capillary 5 min after CA. Dashed lines indicate the vessel contours of first-order capillaries before CA. (Scale bars: 20 μm.) (*C*) The most severe constrictions at the first- and second-order capillaries colocalized with pericytes. The third-order and higher capillaries exhibited moderate constriction. Preconditioning with PPADS mitigated vasoconstriction at the p.a. and first- and second-order capillaries. For the p.a., an unpaired *t* test was used. n/a, not available; $***P < 0.001$. For the other order capillaries, one-way ANOVA with post hoc test was used ($*P < 0.05$). All error bars represent SEM.

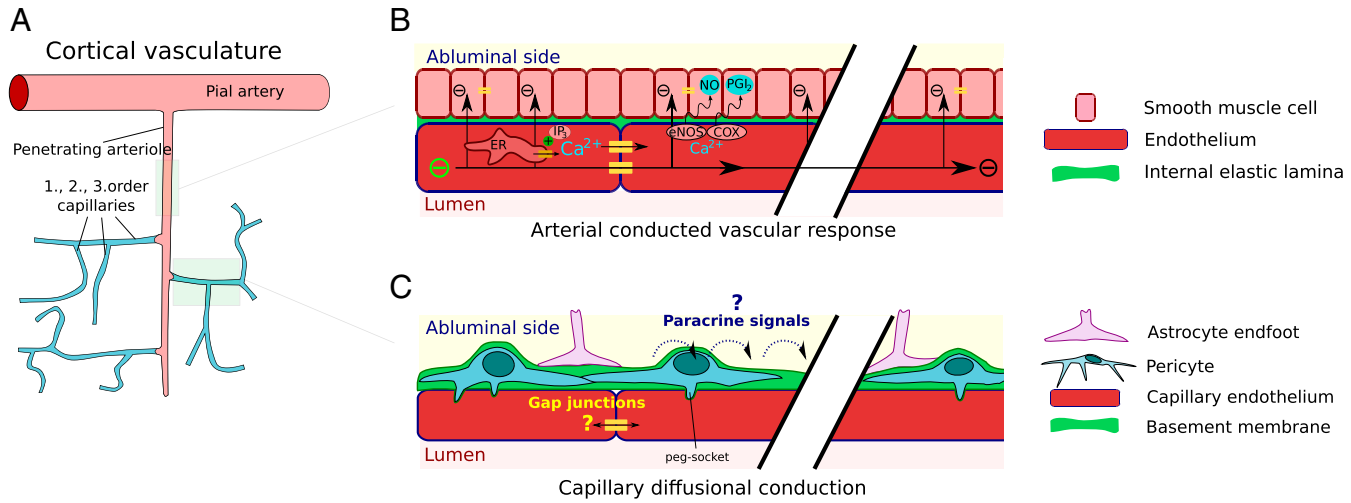

Fig. 7. Possible mechanisms of ATP-puffing-induced dilation and constriction. (*A*) The pial artery and p.a.s consist of endothelium surrounded by smooth muscle cells (light red). As capillaries branch off the p.a., smooth muscle is replaced by pericytes (light blue) with heterogeneous morphologies across first-, second-, and higher-order capillaries (i.e., going from the p.a. to the venous side). (*B*) Fast and long-range conduction along arterioles and arteries via electrical conduction and the local Ca^{2+} wave. (*C*) Observed slow and low-range conduction of vasomotor responses emanating mostly from first- and second-order capillaries seem to involve signaling by diffusion. Both paracrine signaling along astrocyte end-feet and intracellular diffusion along putative gap junctions can be envisioned.

Materials and Methods

Animal Handling. All procedures involving animals were approved by the Danish National Ethics Committee according to the guidelines set forth in the European Council's Convention for the Protection of Vertebrate Animals Used for Experimental and Other Scientific Purposes and were in compliance with the ARRIVE guidelines. Forty NG2-DsRed mice [Tg(Cspg4-DsRed.T1)1Akik/J; Jackson Laboratory] of both sexes were used at 4–7 mo of age. The trachea was cannulated for mechanical ventilation (Minivent type 845; Harvard Apparatus) and catheters were placed into the left femoral artery and vein for the infusion of substances and to monitor blood pressure and blood gases. To ensure that the animals were kept under physiological conditions, we continuously monitored end-expiratory CO_2 (Capnograph type 340; Harvard Apparatus) and blood pressure (pressure monitor BP-1; World Precision Instruments) and assessed blood gases in arterial blood samples twice during each experiment (pO_2, 95–110 mmHg; pCO_2, 35–40 mmHg; pH, 7.35–7.45) using an ABL 700Series radiometer. Body temperature was maintained at 37 °C using a rectal temperature probe and heating blanket (TC-1000 Temperature Controller; CWE).

The experimental setup involved gluing the skull to a metal plate with cyanoacrylate gel (Loctite Adhesives). A 4-mm-diameter craniotomy was drilled, centered 0.5 mm behind and 3 mm to the right of the bregma over the sensory barrel cortex region. After removing the dura, the preparation was covered with 0.75% agarose gel (type III-A, low EEO; Sigma-Aldrich), moistened with artificial cerebrospinal fluid (aCSF; NaCl 120 mM, KCl 2.8 mM, $NaHCO_3$ 22 mM, $CaCl_2$ 1.45 mM, Na_2HPO_4 1 mM, $MgCl_2$ 0.876 mM, and glucose 2.55 mM; pH 7.4), and kept at 37 °C. For imaging experiments, part of the craniotomy was covered with a glass coverslip that permitted the insertion of electrodes and pharmacological interventions.

The mice were anesthetized by i.p. injection of a mixture of ketamine (60 mg/kg) and xylazine (10 mg/kg) and administered supplemental doses (30 mg/kg) of ketamine every 20 min. Upon completion of all surgical procedures, the anesthesia was switched to continuous i.v. infusion with α-chloralose (33% wt/vol; 0.01 mL/10 g/h). At the end of the experimental protocol, the mice were killed by i.v. injection of 0.05 mL pentobarbital followed by cervical dislocation.

Whisker-Pad Stimulation. The mouse sensory barrel cortex was activated by stimulation of the contralateral ramus infraorbitalis of the trigeminal nerve using a set of custom-made bipolar electrodes inserted percutaneously. The cathode was positioned relative to the hiatus infraorbitalis (IO), and the anode was inserted into the masticatory muscles (45). Thalamocortical IO stimulation was performed at an intensity of 1.5 mA (ISO-flex; A.M.P.I.) for 1 ms in trains of 20 s at 2 Hz.

Micropipette Puffing. The glass micropipettes for puffing were produced by a pipette puller (P-97; Sutter Instrument) with a resistance of 3–3.5 MΩ. The pipette was loaded with a mixture of 10 μM Alexa 594 and active substances to visualize the pipette under the two-photon microscope. Guided by the two-photon microscopy, the pipette was inserted into the cortex and the vasculature approached 100–200 μm below the surface. The distance between the pipette tip and vasculature was 30–50 μm (Fig. 2*A*). Substances were puffed for ∼200 ms using an air pressure of ∼15 psi in the pipette. The pipette tip was placed randomly near the p.a. or first- or second-order capillaries and the dye spread very quickly (∼160 μm/s). Within one to two frame acquisition times the "red cloud" covered both the arteriole and the capillaries, and the background returned to normal ∼20 s after puffing. The vasoresponses were not affected by the concentration of ATP at different distances (Fig. S2).

Two-Photon Imaging. FITC-dextran (2% wt/vol, molecular weight 70,000, 50 μL; Sigma-Aldrich) was administered into the femoral vein to label the blood plasma. Experiments were performed using a commercial two-photon microscope (Femto3D-RC; Femtonics Ltd.) and a 25 × 1.0 N.A. water-immersion objective. The excitation wavelength was set to 900 nm. The emitted light was filtered to collect red and green light from DsRed (pericytes) and FITC-dextran (vessel lumen). The frame size was typically 400 × 400 pixels (370 ms per frame). x–y time series were taken to image pericytes and blood vessels during stimulation or micropipette puffing. Our earlier studies (3) used a frame rate of 5.9 Hz, but due to the properties of the instrument we used a frame rate of 2–3 Hz in the present study. The lower frame rate provided excellent spatial resolution of the CVRs in an ensemble of small blood vessels at the same time. However, this time resolution did not allow us to obtain robust information about the latency time to 10% of the response. Therefore, in this study we used the time latency to 50% of the response.

Image Analysis. The analytical software was custom-made using MATLAB. An averaged image over time from green channel was plotted. A rectangular ROI with width of 4 μm was drawn perpendicularly across the vessel longitude (Fig. 1*A*). To minimize the interference with the black shadows of red blood cells and minor vibration of the cortex, the rectangular ROI was averaged by projection into one line for each frame, representing the profile of the vessel segment at this frame. The profile line was plotted as a 2D image with the *x* axis as number of frames (Fig. 1*C*, *Upper*). An active contour algorithm (Chan–Vese segmentation) was used to find the edges of the vessel, which are indicated by the red curves (46, 47), and the time course of the measured diameter was calculated according to the distance between the upper and lower red curves (Fig. 1*C*, *Lower*). Responding capillaries were defined as those with a change of more than 2% of the initial vessel diameter. The vessel response amplitude was defined as the highest peak amplitude after

stimulation/puffing. The response latency was defined as the latency of half-maximal amplitude.

Drug Application. Upon completion of all surgical procedures, FITC-dextran (FD2000S; Sigma-Aldrich) was injected i.v. through the femoral vein catheter to label blood serum and visualize the vasculature under the two-photon microscope (green color). In the micropipette ATP puffing study, the puffing substance was a mixture of 10 μM Alexa Fluor 594 (A-10438; Life Technologies; red color) and 1 mM ATP (A9187; Sigma-Aldrich) dissolved in aCSF. The same method was used for the ATPγS (A1388; Sigma-Aldrich), UTP (U6875; Sigma-Aldrich), and αβ-methylene-ATP (M6517; Sigma-Aldrich) studies. In the preconditioned ATP puffing study using P2 receptor antagonist PPADS (P178; Sigma-Aldrich), aCSF containing 0.5 mM PPADS was used to superfuse the exposed cortex immediately after the dura mater was removed and to prepare both agarose and bathing fluid for the cranial window during imaging. ATP puffing experiments occurred after at least 2 h of PPADS exposure. The same procedure for PPADS application and exposure was used in the subset of experiments in which cardiac arrest and cerebral ischemia was induced by i.v. application of 0.05 mL (200 mg/mL) pentobarbital.

Statistical Analysis. Responses are presented as mean ± SEM. *P* values are from one-way ANOVA with Tukey–Kramer post hoc test or unpaired Student's *t* tests, as appropriate. $P \leq 0.05$ was considered significant. All statistical analyses were performed using MATLAB.

ACKNOWLEDGMENTS. We thank Krzysztof Kucharz for his inspiring advice and professional help with polishing figures and videos and Alexey Brazhe for his kind help with improving the algorithm for video analysis. This study was supported by the Lundbeck Foundation Research Initiative on Brain Barriers and Drug Delivery, the NOVO-Nordisk Foundation, the Danish Medical Research Council, and a Nordea Foundation Grant to the Center for Healthy Aging.

1. Abbott NJ, Patabendige AA, Dolman DE, Yusof SR, Begley DJ (2010) Structure and function of the blood-brain barrier. *Neurobiol Dis* 37:13–25.
2. Sakadžić S, et al. (2014) Large arteriolar component of oxygen delivery implies a safe margin of oxygen supply to cerebral tissue. *Nat Commun* 5:5734.
3. Hall CN, et al. (2014) Capillary pericytes regulate cerebral blood flow in health and disease. *Nature* 508:55–60.
4. Gould IG, Tsai P, Kleinfeld D, Linninger A (2017) The capillary bed offers the largest hemodynamic resistance to the cortical blood supply. *J Cereb Blood Flow Metab* 37: 52–68.
5. Peppiatt CM, Howarth C, Mobbs P, Attwell D (2006) Bidirectional control of CNS capillary diameter by pericytes. *Nature* 443:700–704.
6. Kisler K, et al. (2017) Pericyte degeneration leads to neurovascular uncoupling and limits oxygen supply to brain. *Nat Neurosci* 20:406–416.
7. Yemisci M, et al. (2009) Pericyte contraction induced by oxidative-nitrative stress impairs capillary reflow despite successful opening of an occluded cerebral artery. *Nat Med* 15:1031–1037.
8. Biesecker KR, et al. (2016) Glial cell calcium signaling mediates capillary regulation of blood flow in the retina. *J Neurosci* 36:9435–9445.
9. Mishra A, et al. (2016) Astrocytes mediate neurovascular signaling to capillary pericytes but not to arterioles. *Nat Neurosci* 19:1619–1627.
10. Hill RA, et al. (2015) Regional blood flow in the normal and ischemic brain is controlled by arteriolar smooth muscle cell contractility and not by capillary pericytes. *Neuron* 87:95–110.
11. Fernández-Klett F, Offenhauser N, Dirnagl U, Priller J, Lindauer U (2010) Pericytes in capillaries are contractile in vivo, but arterioles mediate functional hyperemia in the mouse brain. *Proc Natl Acad Sci USA* 107:22290–22295.
12. Wei HS, et al. (2016) Erythrocytes are oxygen-sensing regulators of the cerebral microcirculation. *Neuron* 91:851–862.
13. Attwell D, Mishra A, Hall CN, O'Farrell FM, Dalkara T (2016) What is a pericyte? *J Cereb Blood Flow Metab* 36:451–455.
14. Hartmann DA, et al. (2015) Pericyte structure and distribution in the cerebral cortex revealed by high-resolution imaging of transgenic mice. *Neurophotonics* 2:041402.
15. Mathiisen TM, Lehre KP, Danbolt NC, Ottersen OP (2010) The perivascular astroglial sheath provides a complete covering of the brain microvessels: An electron microscopic 3D reconstruction. *Glia* 58:1094–1103.
16. Wang X, Takano T, Nedergaard M (2009) Astrocytic calcium signaling: Mechanism and implications for functional brain imaging. *Methods Mol Biol* 489:93–109.
17. Fields RD, Burnstock G (2006) Purinergic signalling in neuron-glia interactions. *Nat Rev Neurosci* 7:423–436.
18. Kawamura H, et al. (2003) ATP: A vasoactive signal in the pericyte-containing microvasculature of the rat retina. *J Physiol* 551:787–799.
19. Burnstock G (2016) An introduction to the roles of purinergic signalling in neurodegeneration, neuroprotection and neuroregeneration. *Neuropharmacology* 104: 4–17.
20. Frenguelli BG, Wigmore G, Llaudet E, Dale N (2007) Temporal and mechanistic dissociation of ATP and adenosine release during ischaemia in the mammalian hippocampus. *J Neurochem* 101:1400–1413.
21. Schock SC, et al. (2007) Cortical spreading depression releases ATP into the extracellular space and purinergic receptor activation contributes to the induction of ischemic tolerance. *Brain Res* 1168:129–138.
22. Hossmann KA, Traystman RJ (2009) Cerebral blood flow and the ischemic penumbra. *Handb Clin Neurol* 92:67–92.
23. Ames A, 3rd, Wright RL, Kowada M, Thurston JM, Majno G (1968) Cerebral ischemia. II. The no-reflow phenomenon. *Am J Pathol* 52:437–453.
24. Jensen LJ, Holstein-Rathlou NH (2013) The vascular conducted response in cerebral blood flow regulation. *J Cereb Blood Flow Metab* 33:649–656.
25. Dietrich HH, et al. (2009) Mechanism of ATP-induced local and conducted vasomotor responses in isolated rat cerebral penetrating arterioles. *J Vasc Res* 46:253–264.
26. Kajita Y, Dietrich HH, Dacey RG, Jr (1996) Effects of oxyhemoglobin on local and propagated vasodilatory responses induced by adenosine, adenosine diphosphate, and adenosine triphosphate in rat cerebral arterioles. *J Neurosurg* 85:908–916.
27. Ngai AC, Nguyen TS, Meno JR, Britz GW (2007) Postischemic augmentation of conducted dilation in cerebral arterioles. *Stroke* 38:124–130.
28. Ko KR, Ngai AC, Winn HR (1990) Role of adenosine in regulation of regional cerebral blood flow in sensory cortex. *Am J Physiol* 259:H1703–H1708.
29. Lämmer AB, et al. (2011) The P2 receptor antagonist PPADS supports recovery from experimental stroke in vivo. *PLoS One* 6:e19983.
30. Gaudin A, et al. (2014) Squalenoyl adenosine nanoparticles provide neuroprotection after stroke and spinal cord injury. *Nat Nanotechnol* 9:1054–1062.
31. Krueger M, Bechmann I (2010) CNS pericytes: Concepts, misconceptions, and a way out. *Glia* 58:1–10.
32. Shih AY, et al. (2012) Two-photon microscopy as a tool to study blood flow and neurovascular coupling in the rodent brain. *J Cereb Blood Flow Metab* 32:1277–1309, and erratum (2013) 33:319.
33. Hill J, Rom S, Ramirez SH, Persidsky Y (2014) Emerging roles of pericytes in the regulation of the neurovascular unit in health and disease. *J Neuroimmune Pharmacol* 9: 591–605.
34. Grant RI, et al. (2017) Organizational hierarchy and structural diversity of microvascular pericytes in adult mouse cortex. *J Cereb Blood Flow Metab* 271678X17732229.
35. Masino SA, et al. (2002) Modulation of hippocampal glutamatergic transmission by ATP is dependent on adenosine a(1) receptors. *J Pharmacol Exp Ther* 303:356–363.
36. Thyssen A, et al. (2010) Ectopic vesicular neurotransmitter release along sensory axons mediates neurovascular coupling via glial calcium signaling. *Proc Natl Acad Sci USA* 107:15258–15263.
37. Longden TA, et al. (2017) Capillary K^+-sensing initiates retrograde hyperpolarization to increase local cerebral blood flow. *Nat Neurosci* 20:717–726.
38. Chen BR, Kozberg MG, Bouchard MB, Shaik MA, Hillman EM (2014) A critical role for the vascular endothelium in functional neurovascular coupling in the brain. *J Am Heart Assoc* 3:e000787.
39. Domeier TL, Segal SS (2007) Electromechanical and pharmacomechanical signalling pathways for conducted vasodilatation along endothelium of hamster feed arteries. *J Physiol* 579:175–186.
40. Filosa JA, et al. (2006) Local potassium signaling couples neuronal activity to vasodilation in the brain. *Nat Neurosci* 9:1397–1403.
41. Garland CJ, Dora KA (2017) EDH: Endothelium-dependent hyperpolarization and microvascular signalling. *Acta Physiol (Oxf)* 219:152–161.
42. Liu S, Agalliu D, Yu C, Fisher M (2012) The role of pericytes in blood-brain barrier function and stroke. *Curr Pharm Des* 18:3653–3662.
43. Flores-Soto E, et al. (2012) PPADS, a P2X receptor antagonist, as a novel inhibitor of the reverse mode of the Na^+/Ca^{2+} exchanger in Guinea pig airway smooth muscle. *Eur J Pharmacol* 674:439–444.
44. Chen BC, Lee CM, Lin WW (1996) Inhibition of ecto-ATPase by PPADS, suramin and reactive blue in endothelial cells, C6 glioma cells and RAW 264.7 macrophages. *Br J Pharmacol* 119:1628–1634.
45. Norup Nielsen A, Lauritzen M (2001) Coupling and uncoupling of activity-dependent increases of neuronal activity and blood flow in rat somatosensory cortex. *J Physiol* 533:773–785.
46. Chan TF, Sandberg BY, Vese LA (2000) Active contours without edges for vector-valued images. *J Vis Commun Image Represent* 11:130–141.
47. Getreuer P (2012) Chan–Vese segmentation. *Image Process On Line* 2:214–224.